Available online at www.sciencedirect.com
ScienceDirect
Surface & Coatings Technology 202 (2008) 1847–1852
SURFACE & COATINGS TECHNOLOGY
www.elsevier.com/locate/surfcoat

The effect of hot-dipped aluminum coatings on Fe-8Al-30Mn-0.8C alloy

C.W. Su, J.W. Lee, C.S. Wang, C.G. Chao, T.F. Liu *

Department of Materials Science and Engineering, National Chiao Tung University, 1001 Ta Hsueh Road, Hsinchu, Taiwan 30049, ROC

Received 25 May 2007; accepted in revised form 3 August 2007
Available online 17 August 2007

Abstract

The morphology and microstructure of an intermetallic layer formed on the surface of Fe-8Al-30Mn-0.8C alloy by hot-dip aluminization treatment have been examined in detail. The phases present in the coating are unambiguously identified by means of transmission electron microscopy. After aluminization, a two layer coating was formed consisting of an external Al layer and a $(Fe, Mn)_2Al_5$ intermetallic on top of the substrate. The $(Fe,Mn)_2Al_5$ compound has an orthorhombic structure with lattice parameters $a=0.752$ nm, $b=0.667$ nm and $c=0.417$ nm. The activation energy (E_{FeMnAl}) for the growth of such an intermetallic layer is calculated to be 52.7 kJ/mol. These results are different from those observed in aluminized low-carbon steel (E_{Fe}). The difference between E_{FeMnAl} and E_{Fe} is attributed to the alloying elements (Mn) in the present alloy. Environmental salt fog corrosion and high temperature oxidation tests were carried out to examine the corrosion and oxidation resistance. The results indicated that both the corrosion and oxidation resistance of the Fe-8Al-30Mn-0.8C alloy treated by hot-dip aluminization can be significantly increased.

Keywords: Fe-Al-Mn alloy; Hot-dip aluminization; Corrosion; Oxidation; Transmission electron microscopy; TEM

1. Introduction

Fe-Al-Mn alloy is used in some commercial products requiring light weight, ductility and high strength. Although the corrosion resistance of Fe-Al-Mn alloy is higher than that of carbon steel, it is still inferior to that of conventional stainless steel [1–5]. Despite attempts to develop Fe-Al-Mn alloy as a substitute for stainless steel, the alloy's lower corrosion resistance restricts its industrial applications.

Surface coatings have been considered for improving the corrosion resistance of Fe-Al-Mn alloy [6–9]. Taking into account the factors of environmental protection, economy and convenience for mass production, and superior corrosion resistance, hot-dip aluminizing is one of the most practical processes utilized on Fe-Al-Mn alloy. Hot-dip aluminization has been applied to carbon steels, low-alloyed steel, stainless steels and so on. It has been pointed out that an intermetallic layer forms on the surface of the steel substrate during the hot-dip aluminizing process. Such an intermetallic layer dominates the performance of the uncoated material, so that much effort has been made to evaluate its microstructure and characteristics [10–20]. Many investigations have shown that the microstructure of an intermetallic layer is significantly influenced by the chemical composition of the substrate and the coating bath [21,22]. In most studies, either X-ray diffraction or energy-dispersive X-ray spectrometry (EDS) analysis was exclusively used to examine the intermetallic phases. However, it is hard to identify precisely an intermetallic phase by X-ray diffraction due to the complex spectrum and very weak intensities of the peaks obtained from the thin intermetallic layer. Also, the intermetallic phase may exist in a range of compositions rather than having a stoichiometric constitution.

So far, although the intermetallic layers formed on carbon steel during the hot-dip aluminizing process have been extensively examined, at present the corresponding information concerning layers formed on Fe-Al-Mn alloy is unavailable. Therefore, the main purpose of this study is an attempt to inspect in detail and the morphology and microstructure of the intermetallic layer formed on hot-dip aluminized Fe-8Al-30Mn-0.8C alloy by means of transmission electron microscopy (TEM). The activation energy of growth for such an

* Corresponding author. Tel.: +886 3 5712121x55316; fax: +886 3 5713987.
E-mail address: tfliu@cc.nctu.edu.tw (T.F. Liu).

0257-8972/$ - see front matter © 2007 Elsevier B.V. All rights reserved.
doi:10.1016/j.surfcoat.2007.08.011

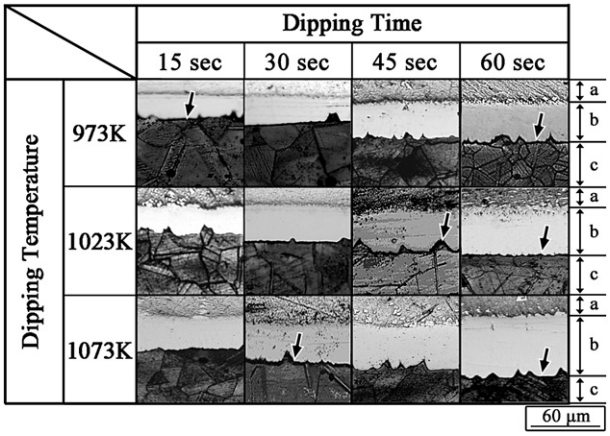

Fig. 1. Cross-sectional optical micrographs of the coating layers formed on the present Fe-Al-Mn alloy after aluminizing at 973 K, 1023 K and 1073 K for various time periods. (a: Al layer; b: intermetallic layer; c: substrate).

intermetallic layer is also evaluated. Finally, after the hot-dip aluminizing process, the corrosion and oxidation resistances are also examined.

2. Experimental procedure

The present alloy, Fe-8wt.%Al-30wt.%Mn-0.8wt.%C, was prepared in a vacuum induction furnace by using 99.5% iron, 99.7% aluminum, 99.9% manganese, and pure carbon powder. After being homogenized at 1523 K for 12 h under a controlled protective argon atmosphere, the ingot was hot-forged and then cold-rolled to a final thickness of 2.0 mm. The sheet was subsequently solution heat-treated at 1373 K for 2 h and rapidly quenched in room-temperature water. The hot-dipped specimens were first cleaned and degreased and then coated with a welding flux consisting of 30% Na_3AlF_6 and 70% NaCl. After the pretreatment, the specimens were immersed in a bath of pure molten aluminum held at 973 K, 1023 K and 1073 K for various time periods.

Optical metallography samples for cross-sectional observations were mounted on bakelite, ground with emery paper, polished with 0.05 μm Al_2O_3 powder and finally etched using a solution of 5% HNO_3 and 95% ethanol. TEM specimens were polished to a thickness of around 40 μm and then argon-ion milled using a Gaton ion-milling machine. These specimens were examined on a JEOL-2000FX scanning transmission electron microscope operating at 200 kV. This microscope was equipped with a linked ISIS 300 energy-dispersive X-ray spectrometer (EDS) for chemical analysis. Quantitative analyses of the elemental concentrations of Fe, Al, and Mn were obtained with the aid of the Cliff–Lorimer ratio thin section method. Elemental depth-profile analyses from the surface of the hot-dip aluminized specimens to the substrate were examined by using LECO-GDS-750A glow discharge spectroscopy (GDS) system. Microhardness measurement for the coating layers was carried out using a Vickers FM7360 microhardness tester under a load of 25 g for 10 s. The ASTM B117 salt fog spray test was used to evaluate the accelerated corrosion performance. The specimens were exposed to a salt fog generated by a 5% sodium chloride solution at 300 K for various times. For the oxidation test, the specimens were heated to 1173 K in ambient air for various times. The oxidation resistances were evaluated by measuring the mass change of the specimens after the oxidation tests. After removing the oxide layer from the specimen, X-ray diffraction (XRD) investigation was carried out to identify the oxide layer by using a Siemens D500 diffractometer.

3. Results and discussion

3.1. Microstructure and phase constitution

Fig. 1 shows a typical multi-layered morphology of the present alloy after immersion in a molten aluminum bath held at 973 K, 1023 K and 1073 K for various time periods. Fig. 1 reveals dark lines appearing at the coating surface interface (between layer “b” and “c”, as indicated by arrows). This is due

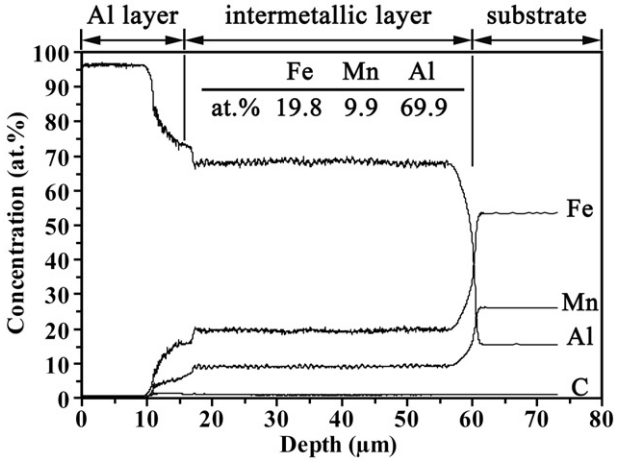

Fig. 2. Concentration–depth profiles for elements in the coating layers formed on the present Fe-Al-Mn alloy after aluminizing at 973 K for 60 s.

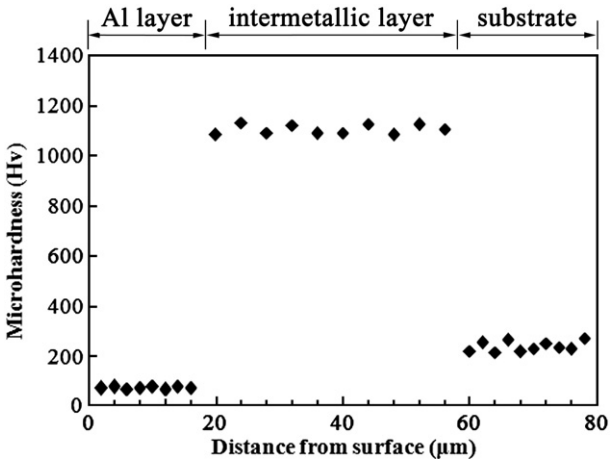

Fig. 3. Microhardness–depth profile of the coating layers formed on the present Fe-Al-Mn alloy after aluminizing at 973 K for 60 s.

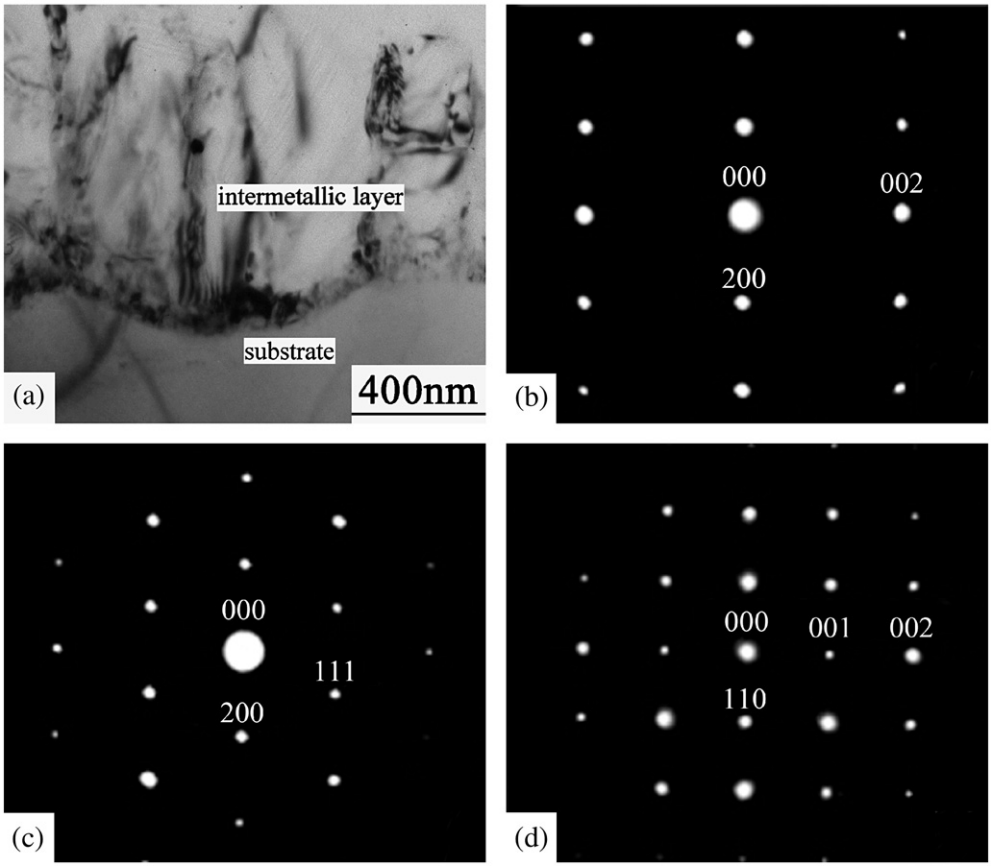

Fig. 4. Cross-sectional transmission electron micrographs of the area close to the interface between the $(Fe,Mn)_2Al_5$ intermetallic layer and the substrate: (a) BF, (b)–(d) three SADPs taken from the intermetallic layer; the zone axes are $[0\bar{1}0]$, $[0\bar{1}1]$ and $[1\bar{1}0]$, respectively.

to the difference of the etching rate between the coating layers and the substrate. In order to observe the coating layers (Al layer and intermetallic layer), prolonged etching time period is necessary. It results in the over-etched substrate, especially on the grain boundaries and the interface between the intermetallic layer and substrate. GDS was used to evaluate the concentration–depth profiles for elements from the outermost surface to the substrate. Fig. 2 exhibits the typical results obtained by GDS, revealing two obvious changes in chemical composition and three regions with uniform constitution. Fig. 2 indicates that these three regions can be considered to be an aluminum layer, the intermetallic layer and the substrate, respectively. Fig. 3 displays the microhardness–depth profile of the coating, showing that the hardness values of the Al layer, intermetallic layer and substrate are about Hv 55, Hv 1100 and Hv 250, respectively. The intermetallic layer with a hardness of Hv 1100

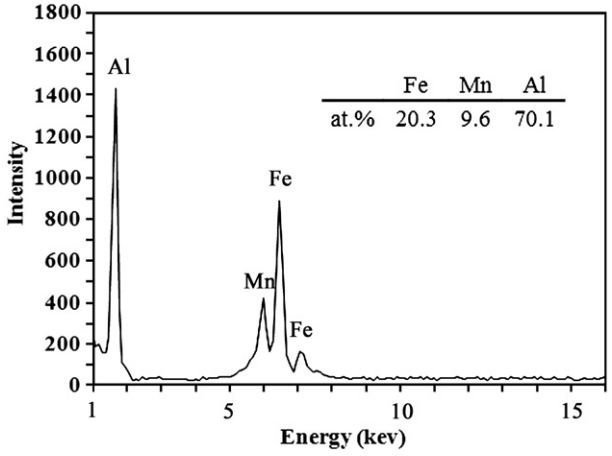

Fig. 5. Typical EDS spectrum taken from the intermetallic layer present in aluminized Fe-Al-Mn alloy.

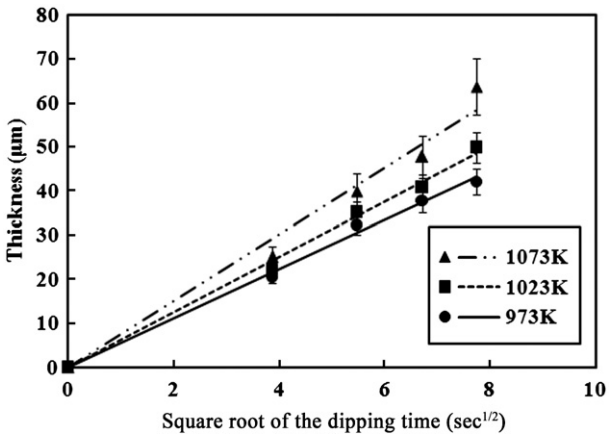

Fig. 6. Relationships between the thickness of the intermetallic layer and the square root of the dipping time at 973, 1023 and 1073 K, respectively.

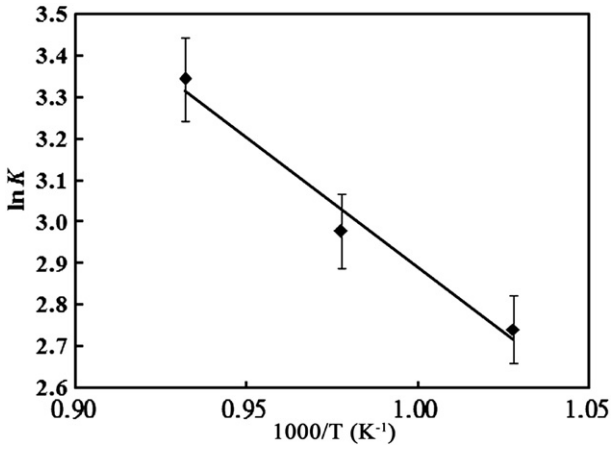

Fig. 7. Plot of the logarithm of the growth-rate constant (ln$K$) against the reciprocal of the dipping temperature (1/T).

is about 40 μm thick, similar to the thickness observed in Fig. 2. The above results imply that the two reacting layers formed on the surface of the present alloy after hot-dip aluminizing at 973 K, are an aluminum layer and an intermetallic layer. The intermetallic phase has a chemical composition of 69.9 at.% Al, 19.8 at.% Fe and 9.9 at.% Mn.

In order to unambiguously identify the intermetallic layer and evaluate its microstructure, TEM examinations were performed. Fig. 4(a) is a cross-sectional bright-field (BF) transmission electron micrograph taken from the area close to the interface between the intermetallic layer and the substrate, revealing a columnar-like morphology of the intermetallic grains. In Fig. 4(a), a dark zone appears at the interface between the intermetallic layer and substrate, which is of the residual welding flux during hot-dip aluminizing. Fig. 4(b)–(d) are three selected-area diffraction patterns (SADPs) taken from the intermetallic layer in Fig. 4(a). The intermetallic phase is (Fe, Mn)$_2$Al$_5$, having an orthorhombic structure with lattice parameters a=0.752 nm b=0.667 nm and c=0.417 nm; the zone axes of Fig. 4(b)–(d) are [010], [011] and [110], respectively. Fig. 5 is a typical EDS spectrum taken from the intermetallic phase shown in Fig. 4. This is consistent with the literature [12,15,19,20,23]. As reported previously, columnar-like Fe$_2$Al$_5$ intermetallic grains, having an orthorhombic structure with lattice parameters a=0.768 nm b=0.640 nm and c=0.420 nm, are observed in aluminized low-alloyed steels [11,12,15,17,19]. The difference of the lattice parameters between (Fe,Mn)$_2$Al$_5$ and Fe$_2$Al$_5$ is attributed to the different atomic radii of Fe and Mn atoms.

Table 1
Area fractions of red/white rust produced in uncoated Fe-Al-Mn alloy, aluminized Fe-Al-Mn alloy and 304 stainless steel after undergoing salt fog spray test for 72, 240 and 1200 h

Materials	Exposing time			
	72 h	240 h	1200 h	
Uncoated Fe-Al-Mn-C Alloy	50%	88%	100%	(Red rust)
Aluminized Fe-Al-Mn-C Alloy	13%	26%	37%	(White rust)
304 stainless steel	7%	19%	31%	(Red rust)

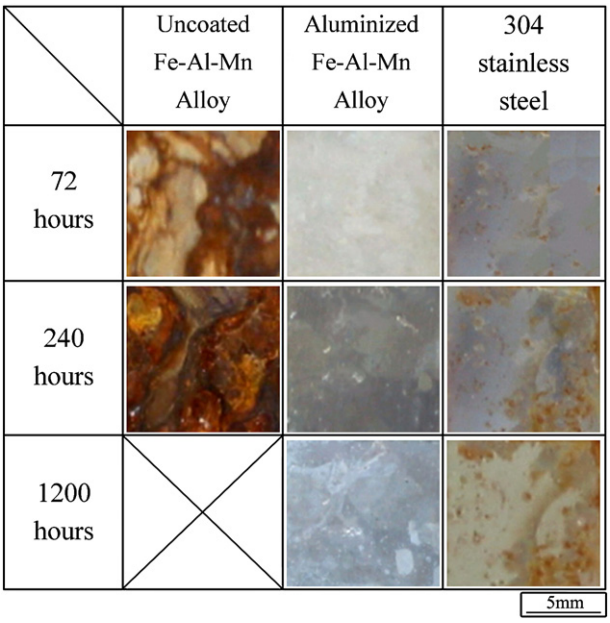

Fig. 8. Optical micrographs of the surface of uncoated Fe-Al-Mn alloy, aluminized Fe-Al-Mn alloy and 304SS after undergoing salt fog spray test.

3.2. Growth kinetics for the (Fe,Mn)$_2$Al$_5$ intermetallic layer

Earlier studies have shown that the growth rate of the Fe$_2$Al$_5$ intermetallic is under diffusion control [12,19]. Thus, the growth equation of an intermetallic layer of thickness x and aluminizing time t is

$$x = Kt^{1/2} \tag{1}$$

and

$$\ln K = \ln K_0 - \frac{E}{RT} \tag{2}$$

where K_0 is a constant, R is the gas constant, T is the absolute temperature and E is the activation energy for the growth of the intermetallic layer. Furthermore, the activation energy (E_{Fe}) for

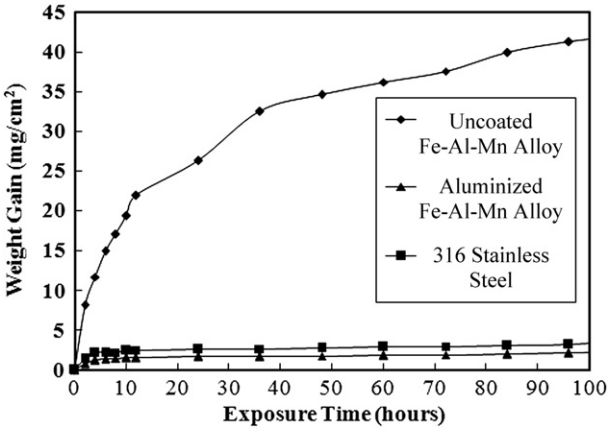

Fig. 9. Plots of the weight gain against the exposure time for 316SS, uncoated Fe-Al-Mn alloy and aluminized Fe-Al-Mn alloy oxidized at 1173 K.

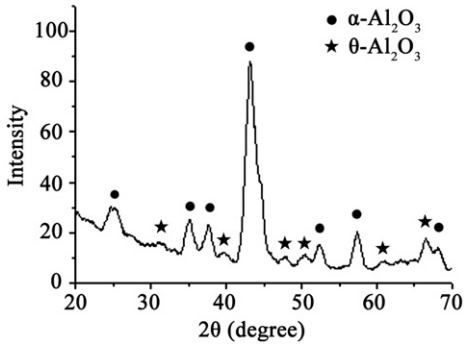

Fig. 10. XRD pattern of the oxide layer formed on the surface of the aluminized Fe-Al-Mn alloy after exposed at 1173 K for 96 h.

growth of the Fe_2Al_5 intermetallic layer formed at the interface of aluminum and carbon steel has been reported to be 155 kJ/mol at temperatures ranging from 943 K to 1073 K [13].

Fig. 6 shows the relationship between the thickness of the $(Fe,Mn)_2Al_5$ layer and the square root of the dipping time at 973, 1023 and 1073 K, respectively. As predicted from Eq. (1), K is determined by the slope of the straight lines in Fig. 6. Fig. 7 shows a plot of ln$K$ against $1/T$. Using Eq. (2), the activation energy (E_{FeMnAl}) for the growth of $(Fe,Mn)_2Al_5$ was calculated to be 52.7 kJ/mol by determining the slope of the nearly straight line in Fig. 7. It is noteworthy that E_{FeMnAl} (52.7 kJ/mol) is much lower than E_{Fe} (155 kJ/mol).

The difference between E_{FeMnAl} and E_{Fe} is attributed to the alloying elements in the present alloy. Akdeniz et al. evaluated the effects of various alloying additions on the growth rate of the intermetallic layer [21,24]. Based on their studies, Mn is discovered to increase the activity coefficient of the Al atom and the growth rate of the intermetallic layer. It appears therefore that the large amount of Mn in this alloy enhances the growth rate of the intermetallic layer, i.e., decreases the activation energy for the growth of the $(Fe,Mn)_2Al_5$ intermetallic layer. Therefore, it is reasonable to propose that the presence of the Mn alloying element in the present alloy may cause an increase in the growth rate of the $(Fe,Mn)_2Al_5$ intermetallic layer, which results from the low activation energy.

3.3. Corrosion and oxidation tests

Salt fog spray test on 304 stainless steel and the present Fe-8Al-30Mn-0.8C alloy with and without hot-dip aluminization were studied. The experimental results of the area fractions of red/white rust produced in these samples after exposed for 72, 240 and 1200 h are shown in Table 1. Fig. 8 reveals the surfaces of the tested samples. Because of the protection in the aluminized Fe-Al-Mn alloy by thick Al-rich coating layers, only white rust (Al_2O_3) but no red rust (Fe_2O_3) was observed on the surface of the specimen after undergoing the salt fog spray test. It can be seen that the corrosion resistance of the present Fe-Al-Mn alloy treated with hot-dip aluminization can be significantly improved and is comparable to that of 304 stainless steel. On the contrary, the uncoated Fe-Al-Mn alloy was totally eroded after undergoing salt fog spray test for 1200 h.

Fig. 9 shows the mass variation of coated and uncoated Fe-Al-Mn alloy as a function of exposure time at 1173 K in ambient air, including 316 stainless steel for comparison purposes. The aluminized Fe-Al-Mn alloy has the lowest weight gain compared with uncoated Fe-Al-Mn alloy and 316 stainless steel. This result shows that the hot-dip aluminizing treatment is capable of remarkably increasing the oxidation resistance of the Fe-Al-Mn alloy.

Previous studies [9,14–16,25,26] in general indicate that the oxidation resistance of Al-rich alloys (in the present study $(Fe,Mn)_2Al_5$) at high temperature is directly related to their Al content, which determines the surface coverage by the aluminum oxide formed. In order to identify the oxide layer, XRD examination was carried out after removing the oxide layer from the specimen. The XRD pattern is shown in Fig. 10, which indicates the forming of Al_2O_3 layer on the surface of the aluminized Fe-Al-Mn alloy after exposed at 1173 K for 96 h. The alumina layer acts as a barrier against oxygen contacting the substrate and provides an additional protection for the alloy from high-temperature oxidation.

4. Conclusions

The coating layers formed on the surface of the Fe-8Al-30Mn-0.8C alloy after hot-dip aluminizing consisted of an aluminum layer and an intermetallic layer. The intermetallic layer was identified to be the $(Fe,Mn)_2Al_5$ phase, which had an orthorhombic structure with lattice parameters $a=0.752$ nm, $b=0.667$ nm and $c=0.417$ nm. The activation energy for the growth of this intermetallic layer at temperatures ranging from 973 K to 1073 K was calculated to be 52.7 kJ/mol. These results are different from those observed in aluminized low-carbon steel. It is reasonable to propose that the presence of the Mn alloying element in the present alloy may lead to a decrease in the activation energy for the growth of the $(Fe,Mn)_2Al_5$ intermetallic layer. The hot-dip aluminizing treatment leads to an obvious increase in the corrosion and oxidation resistances of the Fe-8Al-30Mn-0.8C alloy because of the formation of the $(Fe,Mn)_2Al_5$ layer.

Acknowledgements

The authors are pleased to acknowledge the financial support of this research by the National Science Council, Republic of China under Grant NSC95-2221-E-009-086-MY3. They are also grateful to M.H. Lin for typing the manuscript.

References

[1] M. Ruscak, T.P. Perng, Corrosion 51 (10) (1995) 738.
[2] Y.J. Gau, J.K. Wu, Corros. Prev. Control (April 1997) 56.
[3] X.M. Zhu, Y.S. Zhang, Corrosion 54 (1) (1998) 3.
[4] Y.S. Zhang, X.M. Zhu, Corros. Sci. 41 (1999) 1817.
[5] V.F.C. Luis, M.A. Freitas, E.M. Paula e Silva, Appl. Surf. Sci. 250 (2005) 124.
[6] C.J. Wang, J.W. Lee, T.H. Twu, Surf. Coat. Technol. 163–164 (2003) 37.
[7] J.W. Lee, J.G. Duh, J.H. Wang, Surf. Coat. Technol. 168 (2003) 223.
[8] J.W. Lee, J.G. Duh, S.Y. Tsai, Surf. Coat. Technol. 153 (2002) 59.
[9] J.W. Lee, C.J. Wang, J.G. Duh, J. Mater. Sci. 38 (2003) 3619.
[10] K. Wright, R.N. Wright, G.A. Moore, Scr. Metall. 28 (1993) 501.

[11] K. Bouche, F. Barbier, A. Coulet, Mater. Sci. Eng., A Struct. Mater.: Prop. Microstruct. Process. 249 (1998) 167.
[12] V.N. Yeremenko, Y.V. Natanzon, V.I. Dybkov, J. Mater. Sci. 16 (1981) 1748.
[13] S. Kobayashi, T. Yakou, Mater. Sci. Eng., A Struct. Mater.: Prop. Microstruct. Process. 338 (2002) 44.
[14] A. Aguero, R. Muelas, A. Pastor, S. Osgerby, Surf. Coat. Technol. 200 (2005) 1219.
[15] K. Murakami, N. Nishida, K. Osamura, Y. Tomato, T. Suzuki, Acta Mater. 52 (2004) 2173.
[16] K. Murakami, N. Nishida, K. Osamura, Y. Tomato, Acta Mater. 52 (2004) 1271.
[17] T.S. Shih, S.H. Tu, Mater. Sci. Eng., A Struct. Mater.: Prop. Microstruct. Process. 454–455 (2007) 349.
[18] C.J. Wang, C.C. Li, Surf. Coat. Technol. 177–178 (2004) 37.
[19] T. Sasaki, T. Yakou, K. Mochiduki, K. Ichinose, ISIJ Int. 45 (12) (2005) 1887.
[20] T. Sasaki, T. Yakou, Surf. Coat. Technol. 201 (2006) 2131.
[21] M.V. Akdeniz, A.O. Mekhrabov, T. Yilmaz, Scr. Metall. 33 (12) (1994) 1723.
[22] G.M. Bedford, J. Boustead, J. Mater. Sci. 13 (1978) 253.
[23] H.J. Lamb, M.J. Wheeler, J. Inst. Met. 92 (1963) 150.
[24] M.V. Akdeniz, A.O. Mekhrabov, Acta Mater. 46 (4) (1998) 1185.
[25] D. Wang, Z. Shi, Appl. Surf. Sci. 227 (2004) 255.
[26] Y.Y. Chang, C.C. Tsaur, J.C. Rock, Surf. Coat. Technol. 200 (2006) 6588.